American Mineralogist, Volume 90, pages 725–731, 2005

The true structure of wonesite, an interlayer-deficient trioctahedral sodium mica

TOSHIHIRO KOGURE,[1,*] RITSURO MIYAWAKI,[2] AND YASUYUKI BANNO[3]

[1]Department of Earth and Planetary Science, Graduate School of Science, The University of Tokyo, 7-3-1 Hongo, Bunkyo-ku, Tokyo 113-0033, Japan
[2]Department of Geology, The National Science Museum, 3-23-1 Hyakunin-cho, Shinjuku-ku, Tokyo 169-0073, Japan
[3]Institute of Geoscience, Geological Survey of Japan, AIST, 1-1-1 Higashi, Tsukuba, Ibaraki 305-8567, Japan

ABSTRACT

Wonesite, an interlayer-deficient trioctahedral sodium mica, has been investigated mainly by high-resolution transmission electron microscopy (HRTEM) and X-ray diffraction (XRD) using a Gandolfi camera. The true structure of wonesite is triclinic with a large layer offset, i.e., displacement between the two tetrahedral sheets across the interlayer region, which is partially occupied by sodium ions. The direction and amount of the layer offset is approximately $[1\bar{1}0]$ and 1.25 Å respectively, with unit-cell dimensions of $a = 5.31$, $b = 9.18$, and $c = 9.75$ Å, $\alpha = 96.2$, $\beta = 96.5$, $\gamma = 89.9°$. This interlayer structure, which is similar to that in talc, explains well the exsolution lamellae of talc in wonesite with continuous 2:1 layers. The volume ratio of wonesite and exsolved talc is estimated to be 4:1 to 5:1 from the XRD patterns. Disorder in the directions of the layer offset is occasionally observed in TEM. The interlayer in sodium micas (preiswerkite, paragonite, aspidolite, wonesite, etc.) possesses various amounts of layer offset, depending on the cavity space in the tetrahedral sheet that is primarily determined by the ditrigonal rotation angle.

INTRODUCTION

Wonesite is a rock-forming phyllosilicate discovered first by Spear et al. (1981) from the Post Pond volcanics in Vermont. They reported that the mineral consists of a trioctahedral 2:1 layer and sodium-dominant interlayer cations. Occupancy of cations at the interlayer sites or layer charge is less than but close to 0.5. Although this value does not satisfy the recent definition of mica in which the layer charge must be greater than 0.6, wonesite exceptionally belongs to the mica group (an interlayer-deficient trioctahedral mica) because it does not have swelling or expanding capabilities (Spear et al. 1981; Rieder et al. 1998). The crystal structure of wonesite was reported as monoclinic (*C*2/*m*) with one-layer periodicity. However, the reported β angle is 103.18°, significantly larger than that (ca. 100°) for normal one-layer micas. Single-crystal structure analysis was not completed owing to a fine intergrowth with other phyllosilicates (phlogopite and/or talc), and the origin of this large β angle is not yet clear.

Veblen (1983a, 1983b) investigated the microstructure of wonesite from the same locality using transmission electron microscopy (TEM). His outstanding discovery was fine exsolution lamellae of talc in wonesite. He indicated that wonesite has a greater interlayer occupancy than that calculated from bulk chemical analysis. Interestingly, the boundaries of the two phases are inclined and cross the basal planes of wonesite and talc (Veblen 1983a). Moreover, the 2:1 layers in wonesite and talc appear continuous across the boundaries in his HRTEM image. It is well known that adjacent 2:1 layers in normal micas are interlocked by the presence of the interlayer cations at the cavity space formed by the oxygen hexagonal rings in the tetrahedral sheets. On the other hand, the two adjacent layers are displaced by almost *a*/3 at the interlayer region in talc where no interlayer cations exist (Evans and Guggenheim 1988). Hence continuity of the 2:1 layers across the mica-talc boundaries seems difficult, if the different interlayer structures of the two minerals are preserved.

Recently Kogure et al. (2004) investigated the structure of aspidolite, the Na analogue of phlogopite (previously called sodium-phlogopite), mainly by using HRTEM. They found that the interlayer structure in aspidolite (precisely aluminian aspidolite from its composition) is not the same as that in phlogopite. A large layer offset of about *a*/6, i.e., displacement between the two tetrahedral sheets across the interlayer region (Bailey 1984), is found in aspidolite, which results in a triclinic unit cell (aspidolite-1*A*) and a monoclinic cell (aspidolite-1*M*) depending on the direction of the layer offset relative to that of intralayer shift in the 2:1 layer. Such a large layer offset is ascribed to the small ionic radius of sodium compared to the cavity space in the tetrahedral sheet. Prompted by this result and questions on the reported structure of wonesite as mentioned above, we have investigated the structure of wonesite by HRTEM and XRD. The obtained results indicate that this interlayer-deficient sodium mica also contains a large layer offset, more resembling talc than normal potassium micas.

SAMPLES AND METHODS

Rock fragments containing wonesite from the Post Pond volcanics, Vermont, were obtained from the National Museum of Natural History, Washington, D.C. (catalog no. NMNH 145724) and from Dr. S. Guggenheim, University of Illinois at Chicago. Electron microprobe analyses of wonesite indicated almost the same composition as reported by Spear et al. (1981). Specimens for TEM examination along [*hk*0] directions were prepared by using the method described in Kogure (2002). Platy wonesite crystals obtained from the rock were embedded with epoxy resin between two glass slides. After hardening, the glass slides were cut using a diamond wheel to laths of about 1 mm thickness. The laths were thinned to about 50 μm by mechanical grinding and final thinning was by argon ion milling. HRTEM examination was performed at 200 kV using a JEOL JEM-2010 with a nominal

* E-mail: kogure@eps.s.u-tokyo.ac.jp

0003-004X/05/0004–725$05.00/DOI: 10.2138/am.2005.1791

point resolution of 2.0 Å (C_s = 0.5 mm). High-resolution images were recorded on films at near Scherzer defocus. Successful images recorded on the films were digitized using a CCD camera for image processing. Noisy contrast from amorphous materials on the specimen surfaces was removed using the rotational filtering technique (Kilaas 1998) implemented with Gatan DigitalMicrograph version 2.5 (Kogure and Banfield 1998). Some electron diffraction patterns were collected by using a Hitachi HF-2000 TEM because the specimen can be tilted more (up to ±40°) in the TEM than in the JEM-2010 with a high-resolution pole piece (±20°). Multi-slice image simulation was performed using MacTempas (Total Resolution Co.) to examine whether experimental contrasts were reproduced with the proposed structure models. Mica fragments confirmed as wonesite by electron microprobe analysis were attached to a thin glass fiber for XRD measurements. XRD "powder" patterns were obtained with a Gandolfi camera 114.6 mm in diameter employing Ni-filtered Cu$K\alpha$ radiation. The patterns were recorded on an imaging plate and processed with a Fuji BAS-2500 bio-imaging analyzer and with a computer program by Nakamuta (1999).

Results and discussion

Layer offset in wonesite

TEM examination revealed that intergrowth of wonesite and phlogopite is common in the specimen. Interstratification with chlorite layers was also observed occasionally. Figure 1 shows several filtered HRTEM images from (a) intergrown phlogopite and (b–d) wonesite in the specimen. Our previous papers, e.g., Kogure (2002), can be referred to for interpretation of the HRTEM images of micas. Phlogopite in Figure 1a contains a twin near the top and wonesite in Figure 1d contains a chlorite layer. Note that the (001) basal spacing in wonesite (Fig. 1b–d) is definitely smaller than that in the phlogopite (all images are to the same scale). The difference is about 4%, which corresponds to 10.0 Å and 9.6 Å (Spear et al. 1981) for phlogopite and wonesite, respectively. The contrast in the phlogopite is the same as that of normal trioctahedral micas imaged along one of the [100], [110], [1$\bar{1}$0] and their opposite directions as described in Kogure (2002). If the crystal is sufficiently thin (<10 nm) and the focus is adjusted to near Scherzer defocus (ca. –40 nm in the present study), the contrast for the trioctahedral micas appears as follows: the tetrahedral (T) sheet appears as distinct dark spots separated from each other by b/2 (=4.6 Å). Each dark spot corresponds to two tetrahedra, or a tetrahedral chain extending along the beam direction. The structure in Figure 1a has one-layer periodicity and the two T sheets within a 2:1 layer are not staggered, as indicated by the white lines connecting two adjacent dark spots in the magnified images at the bottom. This indicates that the structure is phlogopite-1M observed down [100] or [$\bar{1}$00] (the intralayer shift is parallel to the electron beam). The contrast of the two T sheets across the interlayer regions are also not staggered, in accordance with the normal phlogopite structure where the layer offset is negligible.

On the other hand, the HRTEM image of wonesite (Fig. 1b) also has no stagger between the two T sheets within a 2:1 layer, but the two T sheets across the interlayer region are considerably staggered. This stagger is never expected from the interlayer structure in normal micas but004). This region is definitely not talc as the basal spacing is greater than that of talc (d_{001} = 9.35 Å) and X-ray chemical analysis by TEM-EDS (Energy Dispersive Spectroscopy) detects sodium and a considerable amount of aluminum from the region. The HRTEM image in Figure 1c taken from another wonesite grain shows different contrast. In this case the two T sheets within a 2:1 layer are staggered but those across the interlayer regions are not staggered. We consider that these different contrasts are not related to different structures

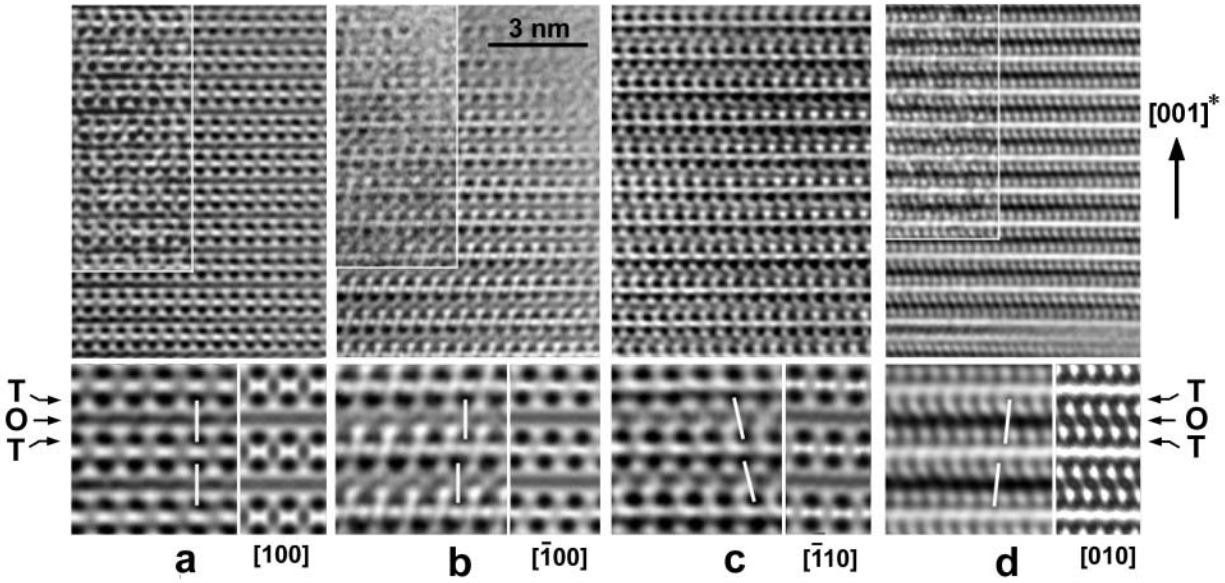

Figure 1. (**a**) Filtered HRTEM image from phlogopite intergrown with wonesite, recorded down [100] or [$\bar{1}$00]. (**b**–**d**) Filtered HRTEM images from different wonesite crystals. The scale is the same for all images. The top-left portion in **a**, **b**, and **d** shows the original, non-filtered image. The bottom part is a magnified image of two unit layers to show the details of the stacking (left side) and simulated contrast (right side) using atomic parameters in Table 1 and the beam direction indicated at the bottom. The specimen thickness and defocus value were assumed to be 2.5 nm and –42 nm (Scherzer defocus) respectively for the simulation. Note that the basal spacing is different between **a** and **b**–**d**, and that the stagger of the two tetrahedral sheets across the interlayer region is observed in **b** and **d**. The experimental contrasts are well reproduced in the simulated images (see the text).

but to different orientations: the layer offset does not appear as stagger in Figure 1c because the offset is almost parallel to the beam direction (this will be examined below by image simulation with the proposed structure model). Finally, an image of a different wonesite grain along one of the [010], [310], or [3$\bar{1}$0] directions is shown in Figure 1d. HRTEM imaging along these directions resolves individual tetrahedra and octahedra which appear as dark spots separated by $a/2$ (= 2.7 Å) in the T and O sheets (Kogure 2002). Here we also recognize the layer offset at the interlayer regions as shown in the magnified image at the bottom-left of the figure.

From these results, it is supposed that wonesite has a large layer offset along one of [110], [1$\bar{1}$0], or their opposite directions and has a triclinic structure similar to aspidolite. To determine the cell dimensions, selected area electron diffraction patterns were acquired from a single wonesite crystal along three principal zone axes (Fig. 2). The pattern in the center is recorded along one of [010], [310], or [3$\bar{1}$0] (or their opposite directions). Diffraction peaks from the exsolved talc described by Veblen (1983a) are not observed in these patterns, as the talc was rapidly amorphized by intense beam radiation before recording the patterns. If we assume the pattern in the center is along the [0$\bar{1}$0] direction, and those upper (specimen tilted by –30° from the position for the pattern in the center) and lower (tilted by +30°) are along [1$\bar{1}$0] and [$\bar{1}\bar{1}$0] respectively, the cell dimensions are calculated to be about a = 5.3, b = 9.2, and c = 9.8 Å, α = 96, β = 96, and γ = 90°. These values have been refined to fit the XRD pattern shown below. The refined dimensions obtained using thirteen non-overlapping peaks are a = 5.31(1), b = 9.18(1), and c = 9.754(6) Å, α = 96.20(8), β = 96.5(1), and γ = 89.9 (2)°. The projection of the ***c***-axis on the basal plane, or lateral displacement between adjacent layers calculated from these cell dimensions, is –0.207***a*** – 0.115***b***. If we assume that the intralayer shift in wonesite is exactly –***a***/3 (this holds true for the 2:1 layers in most trioctahedral micas, see Table 1 in Brigatti and Guggenheim 2002) the layer offset at the interlayer region is 0.126***a*** – 0.115***b***. In other words, the amount of the layer offset is about 1.25 Å and the direction of the offset is almost [1$\bar{1}$0].

Considering this large layer offset, new atomic parameters for wonesite have been derived from those suggested by Spear et al. (1981). In the new model, the structure of the 2:1 layer is preserved and the layer offset is introduced. Sodium ions are assumed to locate at the midpoint of the staggered cavity site. This new structure model has the space group $C\bar{1}$ and the independent sites increase to 11 from 8 in the structure model of Spear et al. (1981) with $C2/m$ symmetry. They are shown in Table 1. The Na and M1 sites are at the position of the symmetry center. Figure 3 shows an experimental XRD pattern from a wonesite crystal taken with the Gandolfi camera (a) and two calculated powder patterns from the structure model of Spear et al. (1981) (c) and our proposed model using the new cell dimensions and atomic parameters in Table 1 (b). The new model explains the experimental pattern far better, indicating that the large layer offset exists in the entire crystal. Modulation of the pattern by the exsolved talc is discussed below. HRTEM contrasts were also simulated from the new structure model, and compared to those in Figure 1. These are shown at the bottom-right of each image in Figure 1. The correspondence is reasonably good if we assume the beam directions indicated in the figure.

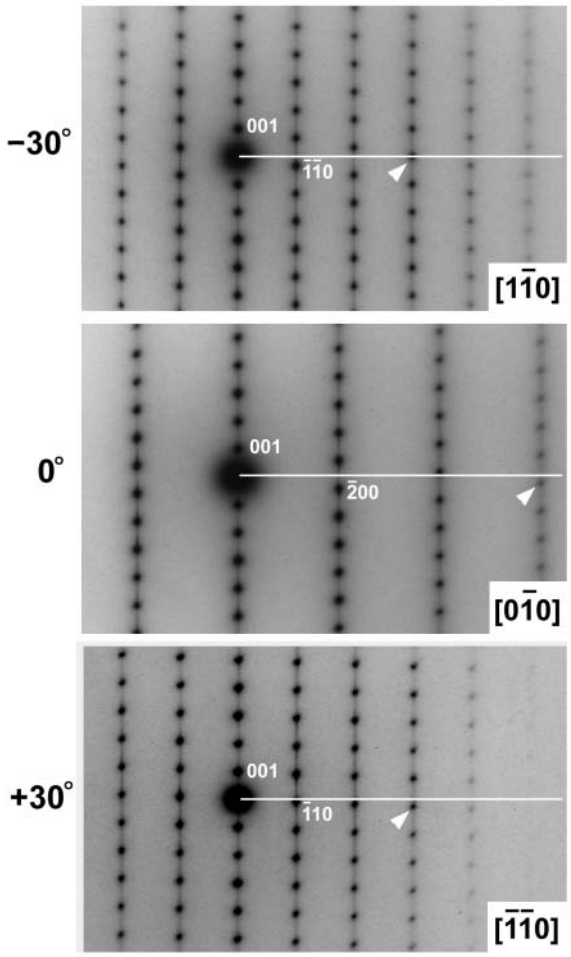

FIGURE 2. Selected area electron diffraction images from a wonesite crystal recorded along three directions. In all images, the ***c****-axis is vertical and horizontal lines are drawn perpendicular to the axis. In normal mica, in which the interlayer shift is close to $a/3$ and the b/a ratio is $\sqrt{3}$, the diffraction spots (060, 330, 600, etc.) as indicated by the white arrowheads should always be on the horizontal lines but they are not in the patterns at the center and bottom.

This result is nearly similar to our previous work for aspidolite (Kogure et al. 2004) but the amount of the shift is considerably larger than that (0.9 Å) in aspidolite. This offset is close to that (1.55 Å) in talc (Perdikatsis and Burzlaff 1981), which explains why the 2:1 layers are continuous across the lamellae boundaries of wonesite and talc (Veblen 1983a). Although the amount of the offset is still different (0.3 Å), the difference may be adjusted around the boundary or the fine talc lamellae may have the same amount of the offset to avoid distortions.

Structural variations in wonesite

Because a pseudo threefold axis runs through the center of the oxygen hexagonal ring, the layer offset in wonesite is expected to occur not only along [1$\bar{1}$0], but also along [110] and [$\bar{1}$00], as observed in aspidolite (Kogure et al. 2004). These different directions of the layer offset were occasionally found in HRTEM

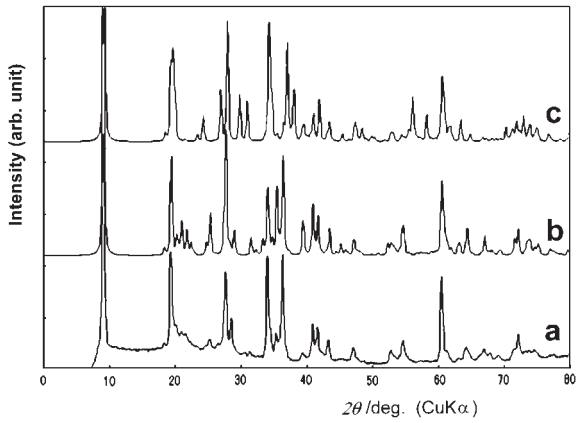

FIGURE 3. (**a**) Experimental XRD pattern from a wonesite crystal acquired with a Gandolfi camera. (**b**) Calculated "powder" pattern with the new cell dimensions and atomic parameters in Table 1. (**c**) Calculated pattern from the model with no layer offset in Spear et al. (1981). For the calculation, a pseudo-Voight function (the same ratio of Gauss and Lorentz functions) with a half-width of 0.35° was assumed for the peak profile. Notice that major peaks in the experimental pattern are reproduced in the calculated pattern in **b**, suggesting existence of a large layer offset.

TABLE 1. New atomic parameters of wonesite derived from those in Spear et al. (1981)

Atom	*x*	*y*	*z*	B	Occupancy
Na	0	0	0	3.0	0.46 Na, 0.09 K
M1	0	1/2	1/2	0.8	0.71 Mg, 0.14 Fe, 0.13 Al
M2	0	0.830	1/2	0.8	0.71 Mg, 0.14 Fe, 0.13 Al
T	0.612	0.137	0.225	0.8	0.78 Si, 0.22 Al
T′	0.612	0.797	0.225	0.8	0.78 Si, 0.22 Al
O1	0.860	0.189	0.158	1.7	1.0 Oxygen
O1′	0.860	0.729	0.158	1.7	1.0 Oxygen
O2	0.560	–0.040	0.158	1.7	1.0 Oxygen
O3	0.643	0.157	0.393	1.2	1.0 Oxygen
O3′	0.643	0.817	0.393	1.2	1.0 Oxygen
O4	0.143	–0.013	0.393	1.2	1.0 Oxygen

images. In Figure 4 the two interlayer regions indicated by the arrowheads show the different stagger directions. As the two T sheets within a 2:1 layer are staggered, the viewing direction is [110] or [1$\bar{1}$0] and consequently the two kinds of the directions for the layer offset must be [1$\bar{1}$0] and [$\bar{1}$00], or [110] and [$\bar{1}$00]. The ordered structure with the [1$\bar{1}$0] offset is the same as that with the [110] offset because the structure has a center of symmetry. However if the direction of the layer offset is ordered along [$\bar{1}$00], the crystal structure is monoclinic with a large interlayer shift by summation of the intralayer shift (*a*/3) and layer offset (ca. *a*/4). Such monoclinic regions were not found during the TEM examination. Furthermore, we calculated the XRD pattern for this monoclinic model and compared experimental X-ray patterns, and no characteristic peaks to indicate this monoclinic domain were found. However, as indicated in Figure 4, layer offset along [$\bar{1}$00] is possible in wonesite. Spear et al. (1981) reported a monoclinic cell with a large β angle (103.18°) by using a four-circle X-ray diffractometer. If the monoclinic structure with [$\bar{1}$00] offset exists, the expected β angle is 103.6°. In this case, the ***c***-axis will be oriented so that the cell edge will be shifted to the opposite direction of the intralayer shift and the layer offset, because the

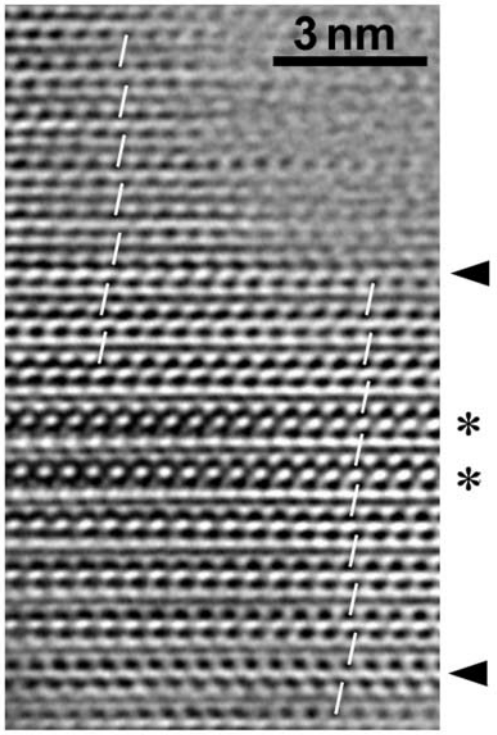

FIGURE 4. Filtered HRTEM image of wonesite, showing intergrowth of phlogopite layers (asterisks) and interlayer regions with different stagger directions (arrows).

total amount of the interlayer shift exceeds *a*/2. Spear et al. (1981) may have measured such a monoclinic structure.

Veblen (1983b) reported two-layer and three-layer polytypes in wonesite. Such polytypes were rare during our observation but a two-layer polytype was found as shown in Figure 5. Although it is insufficient to unambiguously determine the stacking sequence in micas by HRTEM imaging along only one direction (Kogure and Nespolo 1999), a proposed stacking sequence to explain the image contrast is shown in Figure 5c, assuming that intralayer shifts (black arrows) and layer offset (white arrows) are rotated from each other by ± 120°. This stacking sequence is the same as that in paragonite (Lin and Bailey 1984), although the amount of layer offset is largely different (Fig. 5c). Hence this two-layer wonesite structure is monoclinic with space group *C*2/*c*.

Exsolution of talc and the true composition of wonesite

As given above, Veblen (1983a) found exsolution lamellae of talc in wonesite. Similar talc lamellae were also observed in our specimen (Fig. 6a). As Veblen (1983a) reported, the talc lamellae are easily identified with lens-like voids parallel to the (001) plane. To describe wonesite more precisely, we should clarify this lamellae structure. First, the peaks of exsolved talc are determined in the XRD pattern of wonesite. Figure 6b shows an experimental XRD pattern compared to calculated patterns for wonesite and talc. Talc is assumed to contain neither Na nor Al, but Fe content is assumed with a similar Fe/(Mg + Fe) ratio as wonesite. This was confirmed by TEM-EDS analyses, although the analyses were not quantitative owing to selective diffusion of constituent elements in talc, due to the intense convergent beam required for

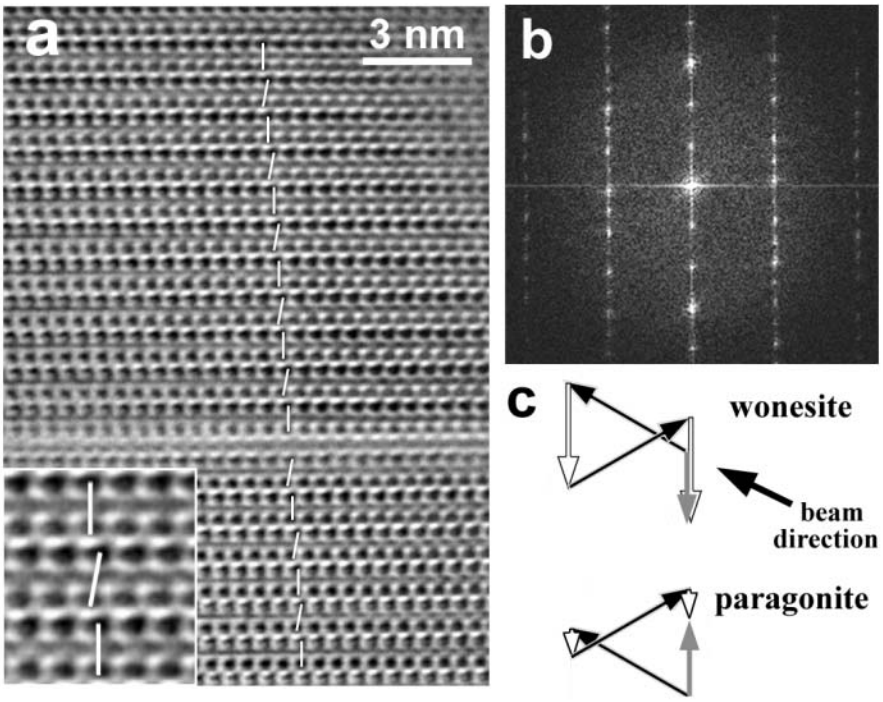

FIGURE 5. (**a**) Filtered HRTEM image of wonesite with two-layer periodicity. A chlorite layer (brucite-like interlayer) exists around the center of the image. A magnified image is at the bottom-left to show the stagger of the T sheets within the 2:1 layers and those across the interlayer regions. (**b**) Fourier transform of **a** to indicate two-layer periodicity. (**c**) Proposed stacking sequence in the two-layer wonesite and that in paragonite for comparison. The black arrows represent the shift between the two T sheets within a 2:1 layer and the white arrows represent the layer offset. The gray arrows indicate the projection of the resultant **c**-axis on the paper.

the analyses. From the comparison, 001 and 003 reflections of talc should occur in the XRD pattern. The 001 reflection of talc forms a shoulder on the 001 peak of wonesite (Fig. 6c) and the 003 reflection forms a separate peak at $2\theta = 28.6°$ (Fig. 6d). We measured five XRD patterns from different wonesite crystals. All patterns showed the 003 peak of talc and the intensity ratio between 003 peaks of wonesite and talc is comparable among the five patterns (Fig. 6e). This suggests that exsolution of talc exists

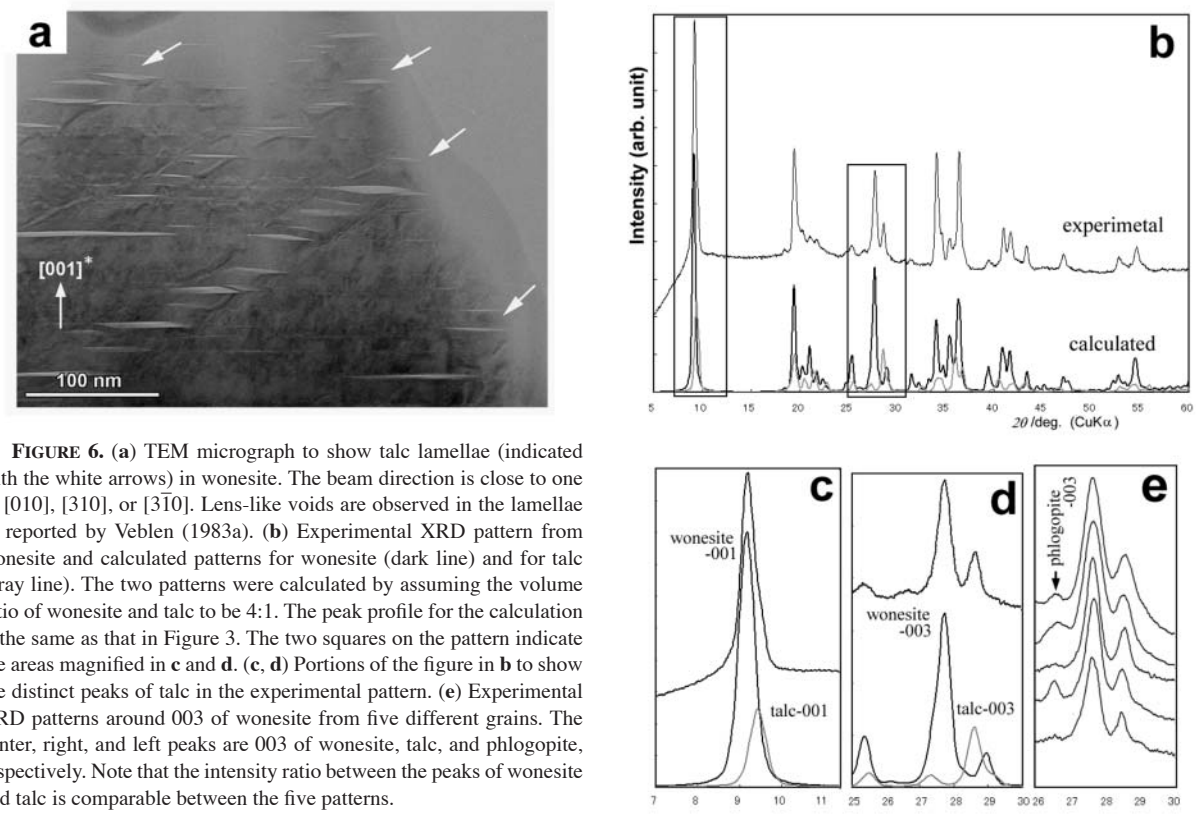

FIGURE 6. (**a**) TEM micrograph to show talc lamellae (indicated with the white arrows) in wonesite. The beam direction is close to one of [010], [310], or [$3\bar{1}0$]. Lens-like voids are observed in the lamellae as reported by Veblen (1983a). (**b**) Experimental XRD pattern from wonesite and calculated patterns for wonesite (dark line) and for talc (gray line). The two patterns were calculated by assuming the volume ratio of wonesite and talc to be 4:1. The peak profile for the calculation is the same as that in Figure 3. The two squares on the pattern indicate the areas magnified in **c** and **d**. (**c**, **d**) Portions of the figure in **b** to show the distinct peaks of talc in the experimental pattern. (**e**) Experimental XRD patterns around 003 of wonesite from five different grains. The center, right, and left peaks are 003 of wonesite, talc, and phlogopite, respectively. Note that the intensity ratio between the peaks of wonesite and talc is comparable between the five patterns.

universally in wonesite. Veblen (1983a) reported that the exsolution lamellae were not found in a wonesite specimen in his TEM examination. However, we believe that the viewing direction was not appropriate to observe the lamellae rather than nonexistence of the exsolution. To observe lamellae clearly, the beam direction must be almost parallel to the lamellae boundaries because the width of the lamellae is very narrow (approximately several tens of nanometers, see Fig. 6a). In our observation, the contrast of the lamellae structure (the lens-like voids) disappeared quickly with specimen tilting of a few tens of degrees.

Second, the volume ratio of wonesite and talc is estimated from the XRD patterns. The square of the structure factor per cell volume calculated for 003 of wonesite and talc is 37.4 and 45.9 $e^2/Å^3$, respectively. For this calculation the composition of talc is assumed to contain 8% Fe at the Mg sites. As discussed below, the composition of wonesite must contain more Al and Na, but the substitution of Si and Mg by Al, and a small increase of the Na content does not change the intensity of 003 appreciably. The intensity ratio between the 003 peaks of wonesite and talc ranges from 4:1 to 3:1 among the five patterns (Fig. 6d). Hence the volume ratio between wonesite and talc is estimated to be about 5:1 to 4:1. Veblen (1983a) estimated the volume ratio to be 3:1 from TEM images and our result is similar. The true chemical composition in wonesite was calculated from these volume ratios and the bulk (wonesite + talc) composition in Spear et al. (1981). If the volume ratio is 5:1, the composition is $(Ca_{0.005}Na_{0.92}K_{0.17})_{1.10}(Mg_{4.25}Fe_{0.75}Mn_{0.004}Cr_{0.008}Ti_{0.07}Al_{0.76})_{5.84}(Al_{1.74}Si_{6.26})_{8.00}O_{20}(OH, F)_4$ and if the ratio is 4:1, the composition is calculated as $(Ca_{0.005}Na_{0.95}K_{0.17})_{1.13}(Mg_{4.21}Fe_{0.75}Mn_{0.004}Cr_{0.008}Ti_{0.07}Al_{0.78})_{5.82}(Al_{1.80}Si_{6.20})_{8.00}O_{20}(OH, F)_4$, where the increased aluminum is distributed to the tetrahedral and octahedral sites as the total number of tetrahedral cations becomes eight.

General principle of the layer offset in sodium micas

From the above results and from our recent work, layer offset is clearly an important parameter in the structure of sodium micas. Here, we discuss the general principle involved in determining the amount of layer offset. The driving force to produce the layer offset is repulsion between facing basal oxygen atoms across the interlayer regions. However, the amount of the layer offset is limited by the interlayer cations to be accommodated in the cavity space of the oxygen hexagonal rings. In the case of potassium micas, the ionic radius of potassium is so large compared to the cavity space, even if the hexagonal rings are not reduced in size by the ditrigonal rotation, that no layer offset occurs. In contrast, sodium ions are small and allow a considerable amount of layer offset if the cavity space is large. The cavity space can be determined by considering the distance between the center of the hexagonal ring and three oxygen atoms that move closer to the center by ditrigonal rotation [d(C-O), see Fig. 7a]. d(C-O) is expressed as:

$$d(\mathrm{C}-\mathrm{O}) = d(\mathrm{O}-\mathrm{O})_b \cdot 2/\sqrt{3} \cdot \sin(60^\circ - \alpha)$$

where $d(\mathrm{O}\text{-}\mathrm{O})_b$ is the average distance between neighboring basal oxygen atoms and α is the ditrigonal rotation angle for the tetrahedral sheet. Here we consider four sodium micas: preiswerkite, paragonite, aspidolite, and wonesite. The rotation angles and layer offsets for preiswerkite and paragonite were reported from their structure analyses (Oberti et al. 1993; Lin and Bailey 1984). Although rotation angles for aspidolite and wonesite are not known, they can be estimated from the compositions using the formula proposed by Weiss et al. (1992). $d(\mathrm{O}\text{-}\mathrm{O})_b$ is easily calculated from the aluminum content of the tetrahedral sites, using the formula and table also reported in Weiss et al. (1992). The rotation angles reported for preiswerkite and paragonite are 20.0° and 16.2° respectively, and those estimated for aspidolite

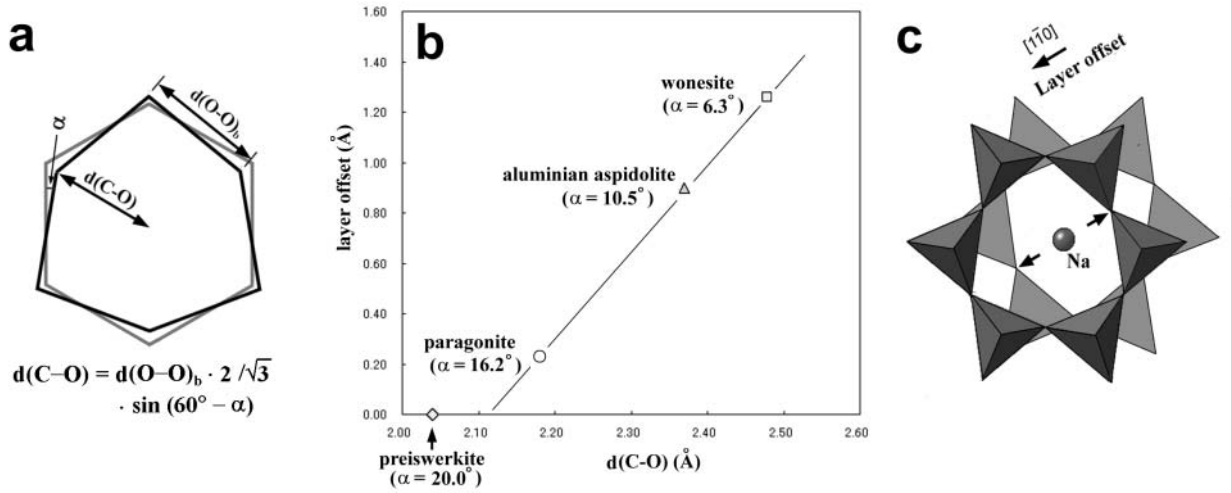

FIGURE 7. (**a**) Definition of d(C-O), the distance between the center of the oxygen hexagonal ring and the closest oxygen atoms, and the equation to calculate d(C-O) from the averaged neighboring O-O distance [$d(\mathrm{O}\text{-}\mathrm{O})_b$] and ditrigonal rotation angle (α). (**b**) The relationship between d(C-O) and the layer offset in four sodium micas. α's for aspidolite and wonesite were calculated from the composition for the 2:1 layer using the formula by Weiss et al. (1992). (**c**) Schematic illustration to show the layer offset between two tetrahedral hexagonal rings across the interlayer region in wonesite. The sodium atom is assumed to be located at the center of the staggered cavity space.

(see Kogure et al. for about the composition) and wonesite (the composition calculated from the volume ratio of 4:1 was used) are 10.5° and 6.3° respectively. Next, *d*(C-O) was calculated from the above equation and plotted with the amount of layer offset for each mica (Fig. 7b). No layer offset exists in preiswerkite (Brigatti and Guggenheim 2002), because of its small cavity space and large α, originating from the complete Tschermak substitution. For the other micas, the amount of layer offset is almost proportional to *d*(C-O) or the cavity space, as shown in Figure 7b.

The location of sodium ions in aspidolite and wonesite is not known and precise structure analyses are required. However, if sodium ions are assumed to be located at the midpoint of the two centers of the staggered hexagonal rings (Fig. 7c), then the two oxygen atoms indicated by the arrows in the figure are closest to the sodium ion based on the layer offset. It is likely that these Na-O distances limit the amount of the layer offset. The closest Na-O distances reported for paragonite (Lin and Bailey 1984), and calculated for aspidolite and wonesite are 2.496, 2.45, and 2.42 Å, respectively. Detailed discussion is not possible because the values for aspidolite and wonesite are derived from several inaccurate and uncertain parameters, e.g., α, the amount of layer offset. However, the shorter Na-O distance in wonesite relative to that in paragonite may reflect the small occupancy of the interlayer cations.

Finally, our investigations have revealed that sodium micas are not the simple analogue of potassium micas as one might expect. Instead, sodium micas belong to a group with a unique character. In most phyllosilicate groups (potassium micas, chlorites, 1:1 phyllosilicates, etc.), the amount of the interlayer shift is a discrete, nearly fixed value (zero, *a*/3 or *b*/3) (Ďurovič 1992). In contrast, the amount of the interlayer shift can be continuous for sodium micas and is strongly dependent on the composition of the 2:1 layer. The obtained results here are fundamental for the identification, structure analysis, and certain applications of sodium micas.

ACKNOWLEDGMENTS

We thank S. Guggenheim (University of Illinois at Chicago) for his comments on the manuscript and for donating a specimen and H. Dong (University of Michigan) for many valuable comments. We also thank P.J. Dunn (Smithsonian National Museum of Natural History) for donating a specimen and T. Takeshige (the University of Tokyo) for preparation of the TEM specimens. Transmission electron microscopy was performed in the Electron Microbeam Analysis Facility of the Department of Earth and Planetary Science, the University of Tokyo.

REFERENCES CITED

Bailey, S.W. (1984) Crystal chemistry of the true micas. In S.W. Bailey, Ed., Micas, 13, 13–60. Reviews in Mineralogy, Mineralogical Society of America, Washington, D.C.

Brigatti, M.F. and Guggenheim, S. (2002) Mica crystal chemistry and the influence of pressure, temperature, and solid solution on atomistic models. In A. Mottana, F.P. Sassi, J.B. Thompson Jr., and S. Guggenheim, Eds., Micas: Crystal Chemistry and Metamorphic Petrology. 46, 1–98. Reviews in Mineralogy and Geochemistry, Mineralogical Society of America, Washington, D.C.

Ďurovič, S. (1992) Layer stacking in general polytypic structures. In A.C.J. Wilson, Ed., International Tables for Crystallography C, 667–680. Kluwer Academic Publishers, Dordrecht, Netherlands.

Evans, B.W. and Guggenheim, S. (1988) Talc, pyrophyllite, and related minerals. In S.W. Bailey, Ed., Hydrous Phyllosilicates (exclusive of micas), 19, 225–294. Reviews in Mineralogy, Mineralogical Society of America, Washington, D.C.

Kilaas, R. (1998) Optical and near-optical filters in high-resolution electron microscopy. Journal of Mineralogy, 190, 45–51.

Kogure, T. (2002) Investigation of micas using advanced TEM. In A. Mottana, F.P. Sassi, J.B. Thompson Jr., and S. Guggenheim, Ed., Micas: Crystal Chemistry and Metamorphic Petrology, 46, 281–312. Reviews in Mineralogy and Geochemistry, Mineralogical Society of America, Washington, D.C.

Kogure, T. and Banfield, J.F. (1998) Direct identification of the six polytypes of chlorite characterized by semi-random stacking. American Mineralogist, 83, 925–930.

Kogure, T. and Nespolo, M. (1999) First occurence of a stacking sequence with (±60°, 180°) rotation in Mg-rich annite. Clays and Clay Minerals, 47, 784–792.

Kogure, T., Banno, Y., and Miyawaki, R. (2004) Interlayer structure in aspidolite, the Na analogue of phlogopite. European Journal of Mineralogy, 16, 891–897.

Lin, C.-Y. and Bailey, S.W. (1984) The crystal structure of paragonite-$2M_1$. American Mineralogist, 69, 122–127.

Nakamuta, Y. (1999) Precise analysis of a very small mineral by an X-ray diffraction method. Journal of the Mineralogical Society of Japan, 28, 117–121.

Oberti, R., Ungaretti, L., Tlili, A., Smith, D.C., and Robert, J.-L. (1993) The crystal structure of preiswekite. American Mineralogist, 78, 1290–1298.

Perdikatsis, B. and Burzlaff, H. (1981) Strukturverfeinerung am Talk $Mg_3[(OH)_2Si_4O_{10}]$. Zeitschrift fur Kristallographie, 156, 177–186.

Rieder, M., Cavazzini, G., D'yakonov, Yu.S., Frank-Kamenetskii, V.A., Gottardi, G., Guggenheim, S., Koval', P.V., Müller, G., Neiva, A.M.R., Radoslowich, E.W., Robert, J.L., Sassi, F.P., Takeda, H., Weiss, Z., and Wones, D.R. (1998) Nomenclature of the micas. Canadian Mineralogist, 36, 905–912.

Spear, F.S., Hazen, R.M., and Rumble, D. (1981) Wonesite: a new rock-forming silicate from the Post Pond volcanics, Vermont. American Mineralogist, 66, 100–105.

Veblen, D.R. (1983a) Exsolution and crystal chemistry of the sodium mica wonesite. American Mineralogist, 68, 554–565.

——— (1983b) Microstructures and mixed layering in intergrown wonesite, chlorite, talc, biotite, and kaolinite. American Mineralogist, 68, 566–580.

Weiss, Z., Rieder, M., and Chemielovà, M. (1992) Deformation and coordination polyhedra and their sheets in phyllosilicates. European Journal of Mineralogy, 4, 665–682.

MANUSCRIPT RECEIVED AUGUST 15, 2004
MANUSCRIPT ACCEPTED OCTOBER 14, 2004
MANUSCRIPT HANDLED BY STEPHEN GUGGENHEIM